Electronic Supplementary Material (ESI) for Soft Matter.
This journal is © The Royal Society of Chemistry 2017

Supplement

High Strain Actuation Liquid Crystal Elastomers Via Modulation of Mesophase Structure

M.O. Saed[ac], R.H. Volpe[a], N. Traugutt[a], R. Visvanathanb, N.A. Clark[b], C.M. Yakacki[a]*

[a] Department of Mechanical Engineering, University of Colorado Denver, Denver, CO80217

[b] Department of Physics, University of Colorado Boulder, Boulder, CO 80309

[c.] Bioengineering Department, The university of Texas at Dallas, Richardson, TX 75080

*E-mail: chris.yakacki@ucdenver.edu

Mesogens

The LC phase formation and the self-assembly in the LCEs is not only dictated by the mesogen structure but also can be influenced by the spacing between the mesogens. In fact, mesogen with the same functional groups and core structures have been used to prepare smectic and nematic LCEs (**Fig S1**). Mesogens with the same functional groups such acrylate (RM82, RM257, and 6OBA) can be used to prepare smectic (6OBA) and nematic LCEs (RM82, RM257).[1-3] This is suggested that functional group may not influence the LC phase formation. Mesogens with the same core structure such as 5Me, 4Me, RM82, and RM257 have been used to prepare smectic (4Me and 5Me) and nematic (RM82 and RM257) main-chain LCEs.[1, 2, 4] The spacing between the mesogens is found to be key element on tuning the LC phase.

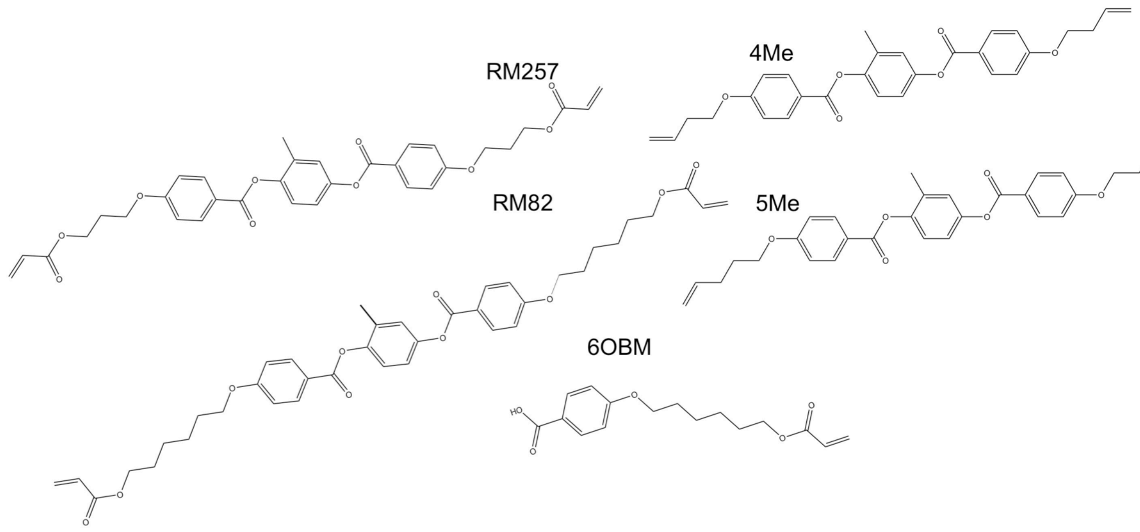

Fig. S1 *Common mesogens used by other research groups to prepare nematic and smectic LCEs. RM257 and RM82 are common nematic mesogens, where 4Me, 5Me, and 6OBA are smectic mesogens,*

Differential scanning calorimetry (DSC) was used to initially characterize the phase transitions in the LCE networks (**Fig. S2**). The first heating scan displayed two or more endothermic wells corresponded to melting temperature and one or two LC transition temperatures. The first (from the left) endothermic well for the all networks is thought to be link to melting temperature of the polymer chain semi-crystallinity. C2 and C6 had an extra endothermic well related to melting temperature. While it is unclear why these materials have two melting transitions, this behavior can be explained based on the self-assembly theory of the nano-scale segregation of ternary incompatible layered. The molecular structure of the mesogen (RM257) contains mesogen core and propylene oxide acrylic terminal chains. Due to structural similarity, the propylene oxide mesogen tail is miscible with C3 spacer. The mesogen tail is not structurally similar (and thus not miscible) with C2 and C6 spacers. Therefore, the resulting LCE of C3 had one melting transition well where C2 and C6 had two melting transition wells. The second heating scan exhibited only LC transitions without melting transition due to slow recrystallization. C2 and C3 revealed one endothermic well, which corresponded to the nematic

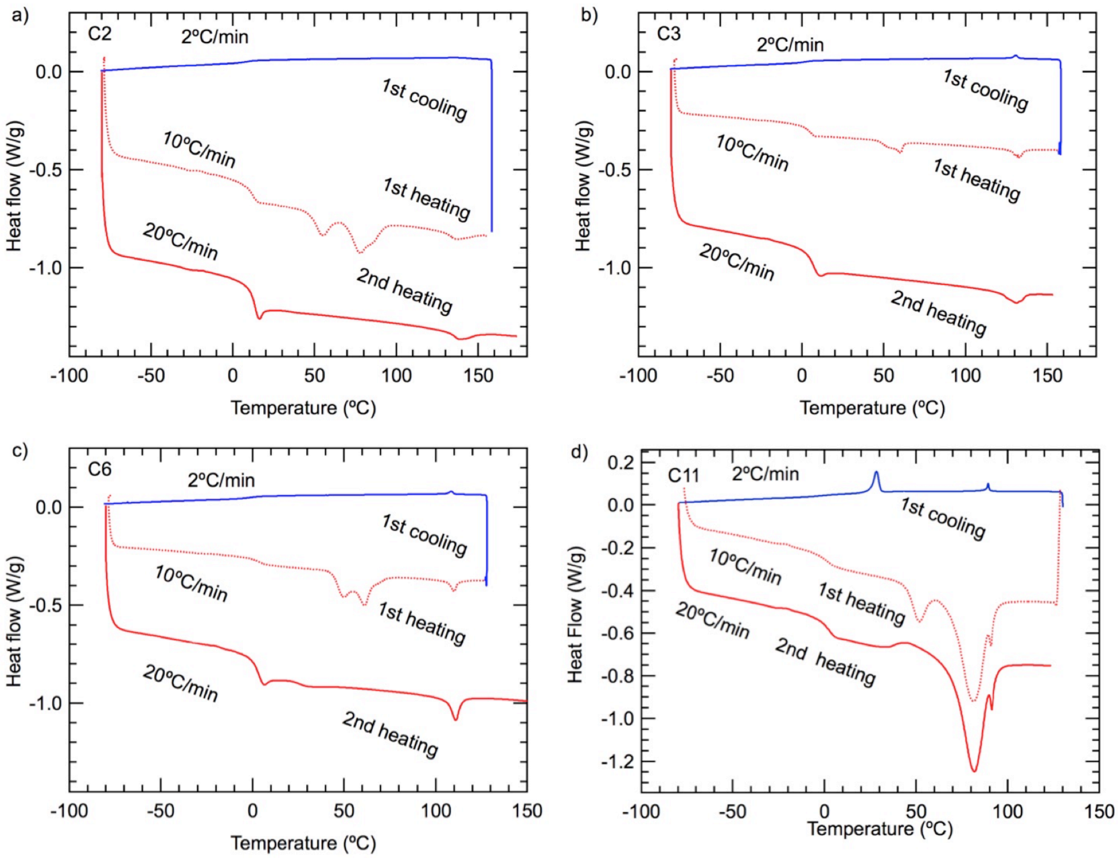

Fig. S2 DSC *heat flows for the C2, C3, C6, and C11. In all plots, the networks were first heated to the isotropic state (T_{NI} + 30°C) at 10°C/min and then cooled to -80°C at 2°C/min. Then heated again at 20°C/min. The melting transition temperatures were measured at the first heating scan where the phase transition temperatures were measured during the second heating scan.*

to isotropic transition. C6 and C11 had an extra endothermic well. This suggested that a smectic phase is present in the materials at lower temperature.

The trend of the transition temperature as a function of the spacer length is shown in **Fig. S3.**The nematic-to-isotropic transition (T_{NI}) increased with decreased spacer length, where the smectic-to-nematic transition temperature (T_{SmC}) showed an opposite trend as it decreased with decreasing the spacer length until completely disappearing at shorter spacers (C2 and C3).

Wide-angle X-ray scattering (WAXS) (1D and 2D) was used next to investigate the influence of spacer length on the mesophase of the materials (**Fig. S4**). C6, C9, and C11 revealed a peak at the smectic region (~0.274596, 0.19485, and 0.187327 A^{-1}, respectively). The intensity of the peak increased with increasing the length of the spacer. Interestingly, the spacing between the layers enlarged linearly with increasing of the length of the spacers. Both C2 and C3 did not form any peak at the smectic region. The presence of crystallinity in each LCE composition is confirmed by WAXS patterns plotted in liner scale **(Fig S4)** and logarithmic scale **(Fig S5).** In 1D plot (Fig S4) each crystallized LCE sample showed 2−5 narrow peaks in the range of ~1.5− ~2.5 A^{-1}, indicating ordered crystalline structures with d-spacing between 4.3 and 2.6 A. These results agree with previously reported study in crystalized LCE materials.[5] The evolution of the mesophase of C6 and C11 was studied as a function of temperature (**Fig. S6 and 7).** C6 exhibited a smectic-to-nematic transition above 50°C, where C11 demonstrated a smectic-to-nematic transition within the tested temperature range.

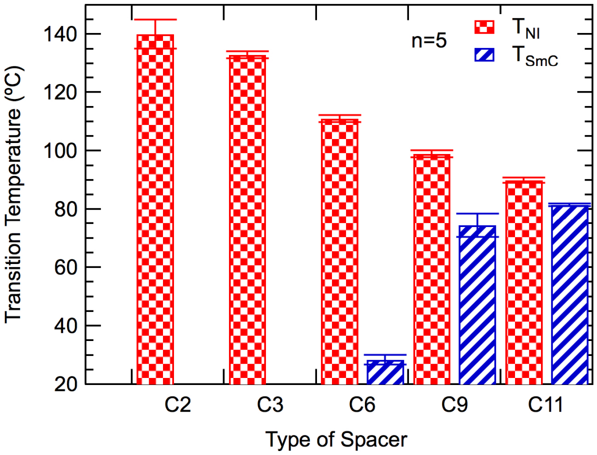

Fig. S3 *LC transition temperatures from the DSC traces of five LCE networks with difference spacer length. Smectic to nematic (T_{SmC}) and nematic to isotropic (T_{NI}) transition temperatures were measured at the second-heating scan at 20°C/min.*

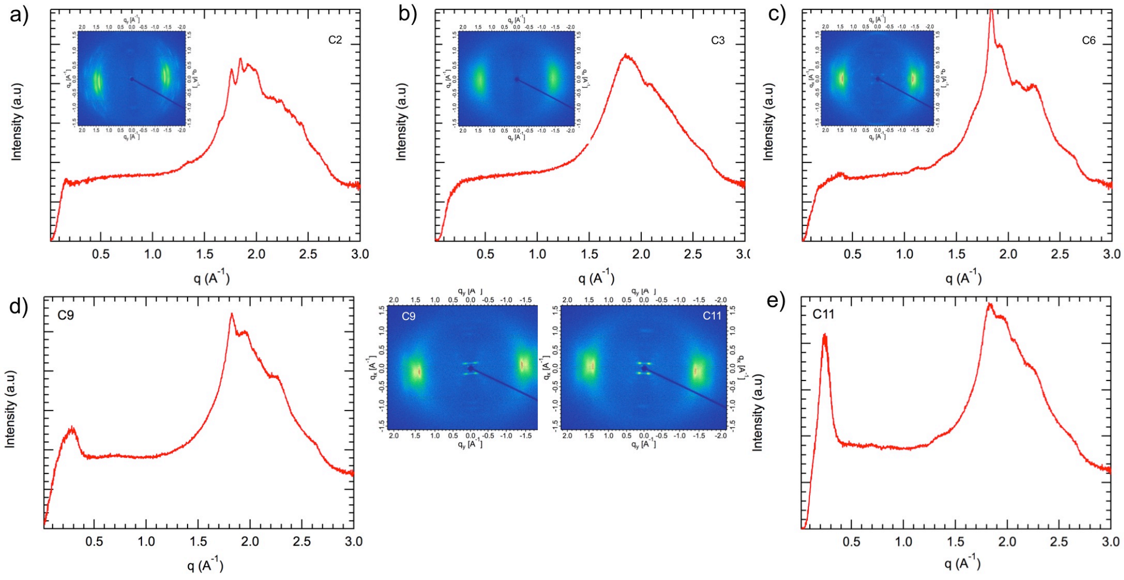

Fig. S4 *1D and 2D WAXS patterns for five LCE networks at room temperature. Diffraction was measured in an aligned monodomain state. Alignment was achieved by stretching the samples to 100% engineering strain before analysis.*

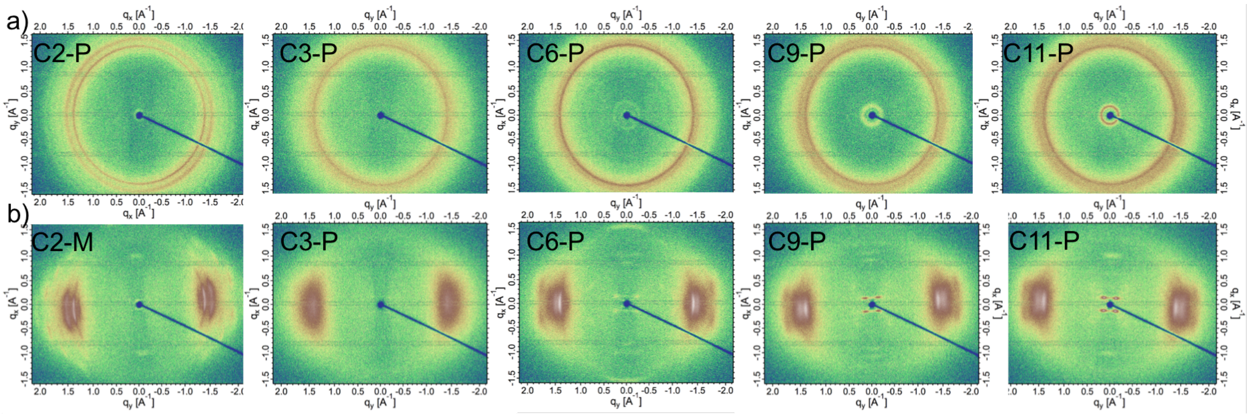

Fig. S5. *2-D WAXS patterns for five LCE networks at room temperature. Diffraction was plotted in the* logarithmic *scale and measured in (a) an unaligned polydomain state and (b) an aligned monodomain state. Alignment was achieved by stretching the samples to 100% engineering strain before analysis.*

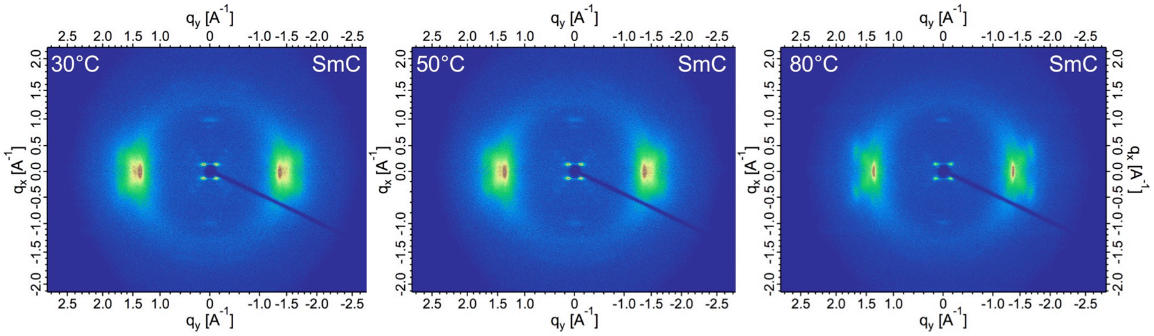

Fig. S6 *Temperature-controlled WAXS analysis of the LCE system using the C11 spacer. Diffraction patterns reveal the present of the smectic c phase over broad range of temperature. All images were taken under 100% engineering strain.*

The advancement of thermo-mechanical properties as a function of spacer length and polymer chain crystallization was studied using dynamic mechanical analysis (DMA). Storage modulus (*E´*) and loss tangent (*tan δ*) traces for the C2 and C3 are shown in **Fig. S8.** A distinct thermo-mechanical behavior for the first heating compared to the rest of the heating scans due to the melting of the semi-crystalline structure during the first heating scans.

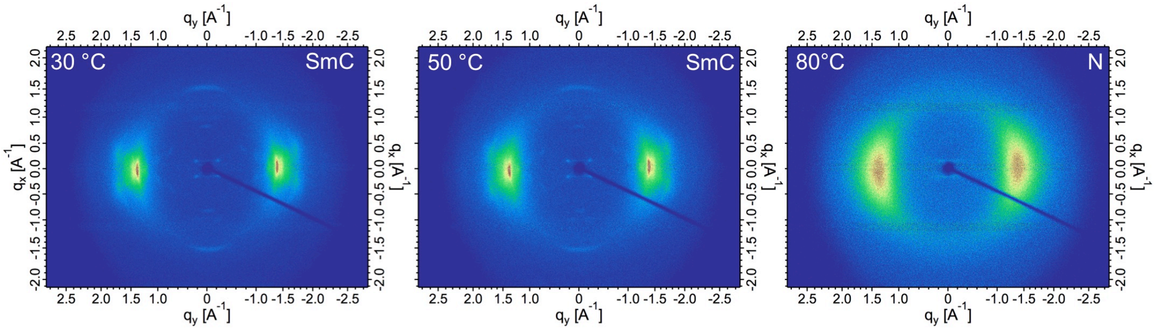

Fig. S7 *Temperature-controlled WAXS analysis of the LCE system using the C6 spacer. Diffraction patterns reveal the transition from a smectic C to nematic orientation when heated above 50℃. All images were taken under 100% engineering strain.*

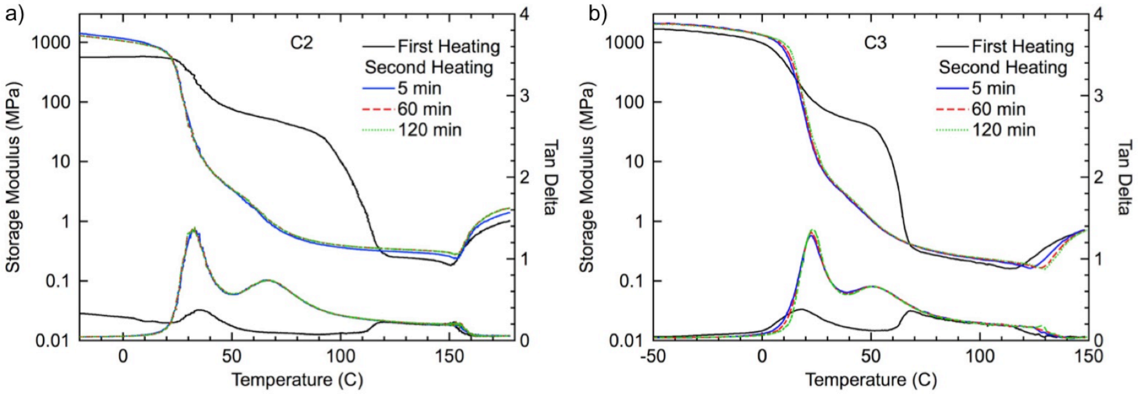

Fig. S8 *Storage modulus (E′) and loss tangent (tan delta) traces for LCE networks with spacer lengths of C2 and C3. Samples were measured at 3°C/min heating rate and 1 Hz frequency in tension. All samples were annealed above* T_{NI} *and allowed to cool at room temperature for 24 hours before the first temperature sweep to allow the semi-crystallinity to fully form. Samples were tested four times and allowed to set isothermally at 25 °C between each sweep for 5, 60, and 120 minutes to show the evolution of the mechanical properties due to polymer chain crystallization.*

The actuation performance of the five LCE networks was measured as a function of temperature (**Fig. S9**). The average actuation performance of semctic LCEs (C6-C11) is higher than nematic LCEs (C2 and C3). This can be attributed to higher enthalpy assisted the LC order in the semctic LCEs.

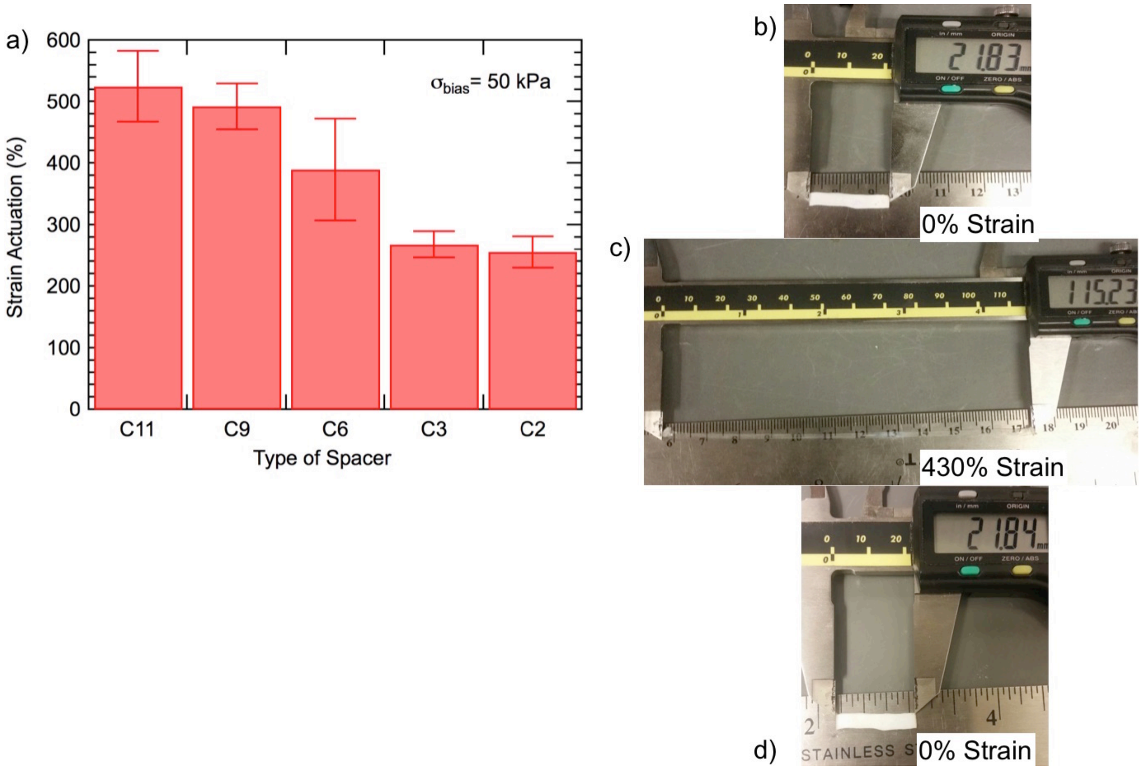

Fig. S9 (a) *Average strain actuation for each network (n=3). Strain actuating was measured from DMA by applying a 50 kPa bias stress at the isotropic state of each sample with cooling rate of 5℃/min. A demonstration of shape memory cycle of C11 is shown. Sample heated above* T_m *and let cool to room temperature (b); the sample stretch to 430% before it crystalized (c); by heating the sample to 100 ℃ sample returns to its original shape.*

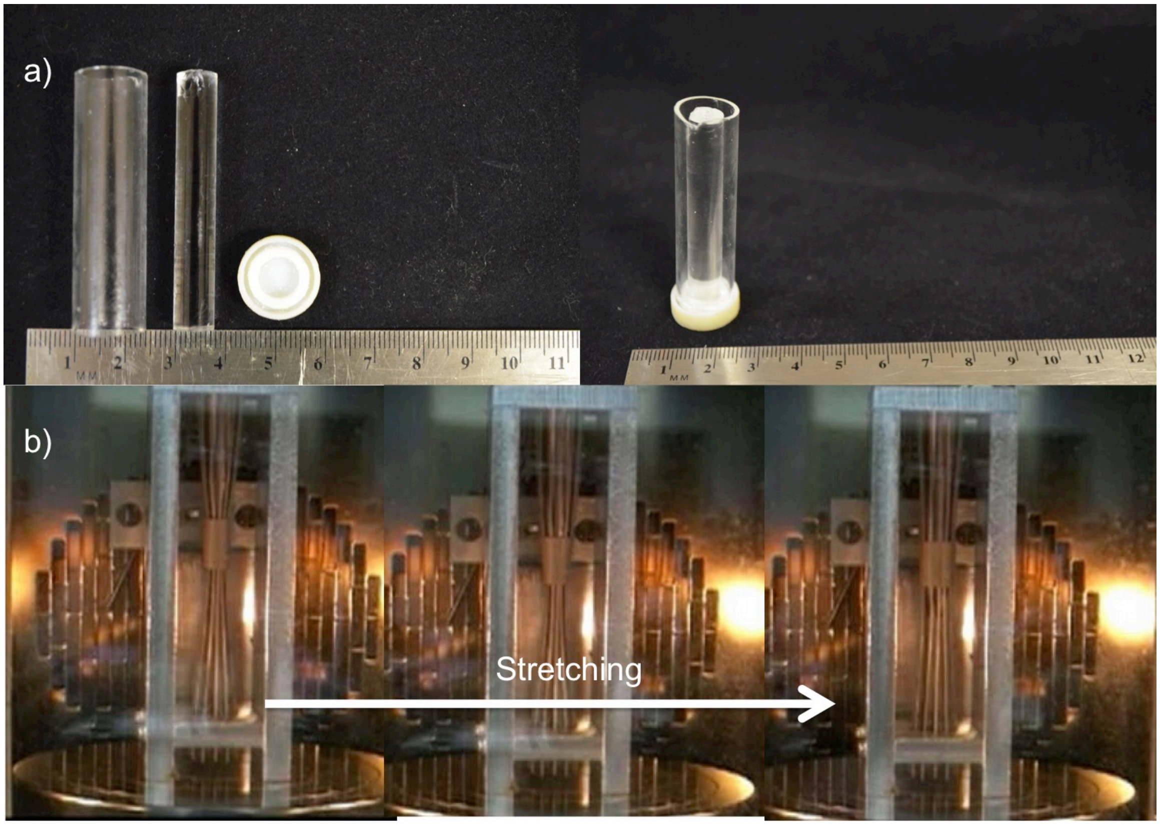

Fig S10. *a) A picture of the cylinder-like mold used for the polymerization of the stent-like LCE samples; b) the stretching process of the stent.*

References

1. T. H. Ware, M. E. McConney, J. J. Wie, V. P. Tondiglia and T. J. White, *Science*, 2015, **347**, 982-984.
2. M. O. Saed, A. H. Torbati, C. A. Starr, R. Visvanathan, N. A. Clark and C. M. Yakacki, *Journal of Polymer Science Part B: Polymer Physics*, 2017, **55**, 157-168.
3. H. P. van Kuringen, G. M. Eikelboom, I. K. Shishmanova, D. J. Broer and A. P. Schenning, *Advanced Functional Materials*, 2014, **24**, 5045-5051.
4. P. T. Mather, I. A. Rousseau and H. Qin, *Journal*, 2009.
5. H. Kim, J. M. Boothby, S. Ramachandran, C. D. Lee and T. H. Ware, *Macromolecules*, 2017, **50**, 4267-4275.